GeoScienceWorld
Lithosphere
Volume 2022, Article ID 6238642, 15 pages
https://doi.org/10.2113/2022/6238642

Lithosphere

Research Article

Research on the Floor Rockburst of Panel Entry under the Mining Influence: A Case Study

Hao Feng,[1] **Xiang Ma**,[2] **Yang Zhao**,[1] **Lishuai Jiang**,[1,3] **Xinglin Wen**,[1] **Qian Cong**,[1] **and Fangtian Wang**[4]

[1]*State Key Laboratory of Mining Disaster Prevention and Control, Shandong University of Science and Technology, Qingdao 266590, China*
[2]*Inner Mongolia Zhongtai Energy Co., Ltd., Yiqi Branch, Ordos 017000, China*
[3]*State Key Laboratory of Mining Response and Disaster Prevention and Control in Deep Coal Mines, Anhui University of Science and Technology, Huainan 232001, China*
[4]*School of Mines, China University of Mining and Technology, Xuzhou 221116, China*

Correspondence should be addressed to Yang Zhao; mrzhao_y@163.com and Lishuai Jiang; lsjiang@sdust.edu.cn

Received 4 April 2022; Accepted 21 May 2022; Published 9 June 2022

Academic Editor: Shaofeng Wang

The stability of the entries of longwall panels is the key to ensure efficient and safe production of coal mines. In order to solve the common problems of floor heave of panel entry in western China, based on a case study, this paper studies the rockburst instability mechanism of entry floor-induced mining by considering the results from a laboratory test, numerical simulations, and field practice. After testing, the coal and rock of the entry are hard and brittle. In particular under the action of impact dynamic load, its dynamic strength is higher and has a positive correlation with the impact pressure, which provides a mechanical premise for subsequent rockburst. Numerical simulation results show that with the mining of the panel, the vertical stress and the maximum principal stress of the floor are mainly concentrated in the coal pillar along the entry, and the area and degree of concentration continue to increase. The horizontal stress is mainly concentrated in the entry floor, which is distributed in the advanced range of the panel. The deformation rate of the entry roof and the ribs is stable, while the floor shows a "mutation" characteristic of not deforming when the panel is far away and suddenly rising when it is closer to the panel. The range of the plastic zone of the roof and floor remains unchanged, the ribs are further deepened, and the mechanical properties of the coal and rock mass are further weakened. The results of this study contribute to providing a reference for the control of surrounding rock of panel entry under similar geological and geotechnical circumstances.

1. Introduction

With the increase in coal mining depth, coal resources in the eastern mining areas in China have been increasingly depleted in recent years, and the overall coal mining layout has gradually shifted to the central and western regions [1]. Although the western mining area is rich in coal resources, the problems of thick coal seam, large burial depth, and complex occurrence cannot be ignored [2, 3]. In particular under the condition of large mining height panels, the surrounding rock deformation of entry, overburden instability caused by mining, and the subsequent dynamic disasters such as rockburst restrict the development of mine in the west [4]. Rockburst, as a sudden rock failure that will pose a serious threat to engineering and human beings, has also happened frequently in some coal seams with low original stresses and shallow-burying condition in western China recently [5]. The Inner Mongolia Autonomous Region is an important coal supply area in western China, with good coal quality and abundant storage. To ensure the safety and efficient production of coal mines, it is essential to maintain the long-term stability of the entry surrounding rock. At present, in many mines in this area, the surrounding rock instability of the entry happened during the mining, and

most of them were characterized by the floor rockburst. Therefore, it is of great significance to study the rockburst instability of the floor during the mining in this area.

Based on the aforementioned background, research studies on the instability of surrounding rock during mining and the mechanism of rockburst have received considerable attention from researchers worldwide. The early rockburst mechanism believed that rockburst was caused by the local stress of coal rock exceeding its strength, but it did not point out under what conditions rockburst will occur. On this basis, Cook et al. [6] and Bieniawski et al. [7] further proposed the stiffness theory and burst tendency theory of rockburst, respectively. Petukhov and Linkov [8] believed that the strain softening of rock after peak strength would lead to rockburst. In addition, the instability theory, the catastrophe theory, and the fractal theory are also used to study the mechanism of rockburst [9, 10]. With the enrichment of engineering practice and methods, some new mechanisms and theories have been proposed one after another. Qi et al. [11] proposed the "three-factor" mechanism of rockburst according to the mining characteristics of coal mines under deep-burying conditions. Song et al. [12] proposed the concept of rockburst active system and established the theory of dissipative structure on the basis of studying entropy equation and dissipative structure. Pan [13] deduced the corresponding critical index of rockburst based on the instability response theory of disturbance response and proposed the instability response theory of rockburst. A large number of engineering studies show that rockburst mostly occur in entries near the panel, and rockburst appears during the panel mining. In response to this problem, scholars have revealed the rockburst mechanism under the influence of mining by means of a laboratory test and numerical simulation and proposed corresponding control methods. Cao et al. [14] studied the rockburst mechanism in the mining of steeply inclined extrathick coal seams using numerical simulation methods and verified them with the field. Kang et al. [15] provided a reference for understanding the mechanism of large-scale roof collapse under rockburst by simulating the longwall panel mining and establishing a physical model. Holub et al. monitored the seismic events caused by the longwall mining and studied the correlation between the particle velocity of the seismic waves and the extent of the roadway damage after rockburst [16].

The above scholars have conducted in-depth research on the mechanism of rockburst and the corresponding control method and have achieved fruitful results. However, under the deep-burying, large mining height, and wide coal pillar conditions, further research is needed on the impact of panel mining on the rockburst instability of the entry floor. In this study, on the basis of the existing research results, this paper takes Hongqinghe Mine as the engineering background and analyzes the evolution characteristics of floor stress and surrounding rock during the mining of entry through on-site investigation, laboratory test, and numerical simulation. The results contribute to providing a reference for rockburst mechanism and control of floor under similar geological and geotechnical circumstances.

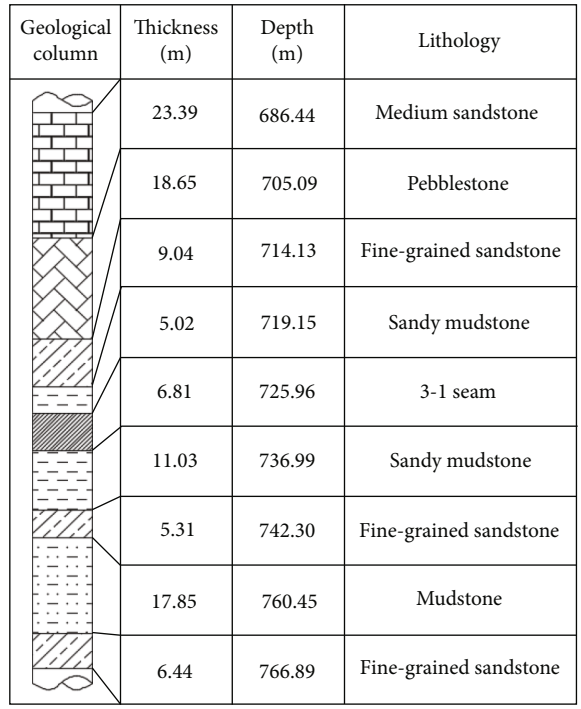

Figure 1: Typical geological column.

2. Case Study

2.1. Engineering Geology Overview of Hongqinghe Mine. The Hongqinghe Mine field is located in the Inner Mongolia Autonomous Region. The mining area has wide and gentle wave-like ups and downs, no fold structure, and no magmatic rock intrusion. Only one normal fault is found in the southwest corner of the mining area, but the drop is relatively small and has no great impact on the mining of the panel. The 3-1 coal seam is the main mining and first mining coal seam. The average thickness of the coal seam is 6.98 m, the average burial depth is 755 m, and the geological conditions of the coal seam are simple. Above the roof are mainly siltstone, medium/fine-grained sandstone, and medium conglomerate, and there is no weak sandstone between each rock layer, forming a composite thick rock layer. The floor is sandy mudstone, mainly semihard rock. Figure 1 shows a typical geological column of the adjacent panel 3103.

2.2. Overview of Rockburst Accidents. The panel adopts fully mechanized mining with large mining height and full-height mining technology. The entry is excavated along the floor of coal seam and adopts a double roadway layout, and a 30 m coal pillar is reserved. Affected by the large mining height, large burial depth, and mining, during the mining of the panel 3101, the headentry (1) of panel 3103 had serious roof fall, floor heave, and rib fall. In order to ensure the safety of production, the headentry (2) of panel 3103 auxiliary was reexcavated on the basis of the 30 m coal pillar, and a 65 m large coal pillar was formed.

However, there are still many rockburst accidents in the entry. At 18:34 on June 14, 2018, a seismic event with an energy of 5.4×10^6 J was monitored at panel 3103. The floor

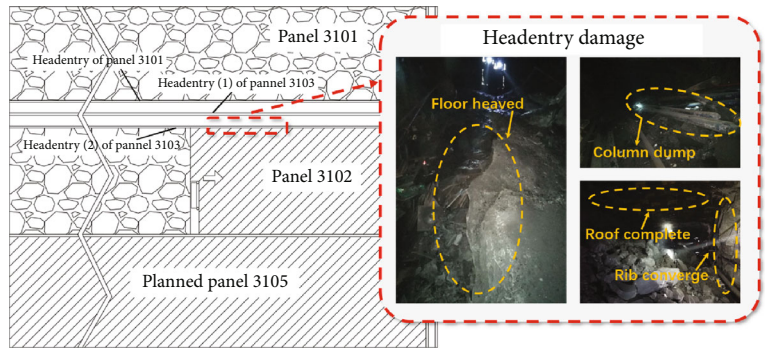

Figure 2: The rockburst accident area and the headentry damage.

heave appeared in the headentry (2) 20 m ahead of the panel accompanied by strong airflow. The safety valve of the hydraulic support is damaged, the metal mesh is broken, and the final width of the floor heave accounts for 2/3 of the entry. At 15:25 on March 19, 2018, a seismic event with an energy of 2.6×10^6 J was monitored during the normal production of the panel 3103, and the panel had an obvious tremor and there was a slight vibration. At 16:10, a strong rockburst event occurred 100 m ahead of the headentry (2) of panel 3103. After the rockburst, the monitored geosound event energy and pulses lasted for nearly an hour and a half, during which there was still a sudden release of large energy. At the same time, the deep stress gauge stress value jumped to 15 MPa. A total of nine hydraulic support safety valves from 115# to 125# were unloaded. The safety valves of the entry support were all damaged due to the pressure. The distance between the floor and the roof was about 1.10 m, and the floor heave volume reached 2.70 m, which is located at the mining side. The rockburst accident area and the headentry damage are shown in Figure 2.

3. Laboratory Test on the Mechanical Behaviors of Coal and Rock Mass under Dynamic and Static Loads

In order to understand the mechanical properties of surrounding rock near the rockburst accident area, the coal mass and floor rock mass near the panel 3103 were sampled. The mechanical properties of coal and rock mass under static load conditions were obtained by a uniaxial compressive test. Subsequently, the split Hopkinson pressure bar (SHPB) test system was used to carry out the impact dynamic load test, and the dynamic characteristics of the coal and rock mass under the impact dynamic load were further obtained.

3.1. Experimental Study on Static Characteristics of Coal and Rock

3.1.1. Specimen Preparation. The 3-1 coal seam and floor rock samples were cored by the SC-200 coring machine and then cut with the SCQ automatic stone cutting machine. Finally, the SCQM automatic cutting and grinding machine was used to grind it to ensure that both ends of the specimen were smooth and flat. According to the method recommended by the International Society for Rock Mechanics (ISRM), the coal and rock specimens were processed into standard cylindrical specimens with a diameter of 50 mm and a height of 100 mm. The processed coal and rock specimens are shown in Figure 3.

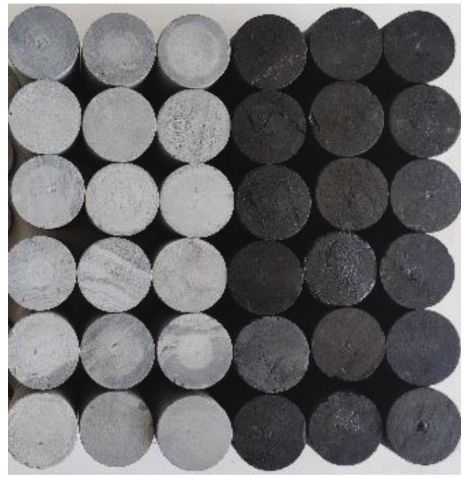

Figure 3: The specimens of coal and rock.

3.1.2. Specimen Preparation. The MTS816 coal and rock mass mechanics test system (Figure 4) was used in the uniaxial compressive test. The system has high performance and stable test accuracy, can collect high and low speed data, and adopts control methods such as force, displacement, axial strain, and lateral strain. The coal and rock specimens were divided into two groups (represented by *C* and *R*, respectively) before the test, with three groups in each group, and the excess specimens were used as spares. The obtained results are averaged in order to discriminate the mechanical properties of coal specimens reasonably and effectively under static conditions [17]. The test scheme is shown in Table 1.

3.1.3. Test Results. The correlation curves of mechanical parameters of coal and rock specimens under uniaxial compressive test are shown in Figure 5. Combined with the detailed test results (Table 2), the maximum value of the

Figure 4: MTS816 electrohydraulic servo rock test system.

Table 1: Static test scheme.

	Coal remark	Rock remark	Dimensions (height × diameter) (mm)
Uniaxial compressive test	C1	R1	50 × 100
	C2	R2	50 × 100
	C3	R3	50 × 100

peak strength of the coal specimen is 24.58 MPa, the minimum value is 17.30 MPa, and the average value is 21.52 MPa. The maximum value of modulus of elasticity is 2.27 GPa, the minimum value is 1.59 GPa, and the average value is 2.03 GPa. The maximum peak strength of the floor rock specimen is 56.30 MPa, the minimum value is 52.44 MPa, and the average value is 54.61 MPa; the maximum modulus of elasticity is 12.59 GPa, the minimum value is 11.58 GPa, and the average value is 12.15 GPa. It can be seen that the coal and rock mass have brittle characteristics, and compared with the coal, the floor rock is harder and the peak strength is higher. In particular, the average modulus of elasticity of floor rock is 6 times that of coal. The critical stress of rockburst under such floor conditions is relatively high. Once rockburst occurs under the action of high stress, the released impact energy will be large, and the impact damage will be more serious.

3.2. Experimental Study on Dynamic Characteristics of Coal and Rock

3.2.1. Specimen Preparation. Larger bulk samples were selected for the coal seam and floor. According to the method recommended by ISRM, a cylindrical specimen with a diameter of 50 mm and an aspect ratio of 1 : 1 is required, and the nonparallelism and nonperpendicularity of the end faces are both less than 0.02 mm. After drilling and grinding, a standard cylindrical specimen with a height of 50 mm and a diameter of 50 mm was obtained. All the coal and rock specimens are shown in Figure 6.

3.2.2. Test System and Test Scheme. The impact dynamic load test adopts the SHPB rock dynamic performance test system (Figure 7). The whole system consists of a stress wave-generating device, a stress transfer mechanism, and a data acquisition and processing device. The dynamic mechanical parameters of the specimen are obtained by processing the stress wave signal generated by the bar. The dynamic load is applied by the impact pressure of the high-pressure nitrogen cylinder. Before setting the impact pressure level, it is necessary to pretest the specimen to obtain the minimum impact pressure at which it will fail. When the specimen begins to have obvious macroscopic damage, the impact pressure at this time is determined to be the minimum impact pressure level, that is, 0.45 MPa. Subsequent impact pressure gradients were then set with 0.05 MPa. The three impact pressure levels set in the test can satisfy the strain rate required for the test. The grouping of coal and rock specimens is the same as above, and the test scheme is shown in Table 3.

3.2.3. Test Results. The specimens were damaged under all loading conditions, and the dynamic stress-strain curves are shown in Figure 8. The curve is quite different from the stress-strain curve under static load. Under the dynamic load, the closed time such as pores and particle spacing inside the specimen is too short, and the characteristics of the compaction stage of microcracks are not obvious. Macroscopically, the compaction stage of the stress-strain curve is missing, and the strain in the failure stage is large. The detailed test results are shown in Table 4. Combined with Figure 8 and Table 4, it can be seen that the impact pressure has a significant impact on the dynamic mechanical behaviors of coal specimens. For the coal specimen, the dynamic strength is 16.8 MPa when the impact pressure is 0.45 MPa. When the impact pressure increased to 0.50 MPa and 0.55 MPa, the dynamic strength of the specimens increased to 27.11 MPa and 32.95 MPa, which increased by 61.3% and 96.1%, respectively. For the rock specimen, the dynamic strength is 60.93 MPa when the impact pressure is 0.45 MPa. When the impact pressure increased to 0.50 MPa and 0.55 MPa, the dynamic strength of the specimens increased to 81.35 MPa and 90.70 MPa, which increased by 33.5% and 48.8%, respectively. With the increase in the impact pressure, the dynamic strength of the specimen increases gradually, showing a distinctive effect of strain rate. After the peak, the springback phenomenon of the rock specimen curve is more significant. Compared with the uniaxial compressive strength under static load, the dynamic strength of the specimen has been improved, and the enhancement degree of the rock specimen is greater than that of the coal specimen, which indicates that the impact of the external impact dynamic load on the floor is more significant.

In conclusion, by testing the mechanical properties of the coal and rock mass specimen under different dynamic and static loading conditions, it can be found that the floor rock of panel 3103 is hard and has brittle characteristics. At the same time, there is a long-term high stress load in the deeply buried environment, so large amount of potential energy is accumulated inside the floor, which provides a prerequisite for the occurrence of the rockburst. Secondly, the coal and rock mass show an effect of strain rate, and its dynamic strength increases with the increase in impact pressure. When a large impact is applied, the hard floor rock becomes the medium for energy accumulation and transfer, which further deteriorates the mechanical conditions at the weak point of the entry.

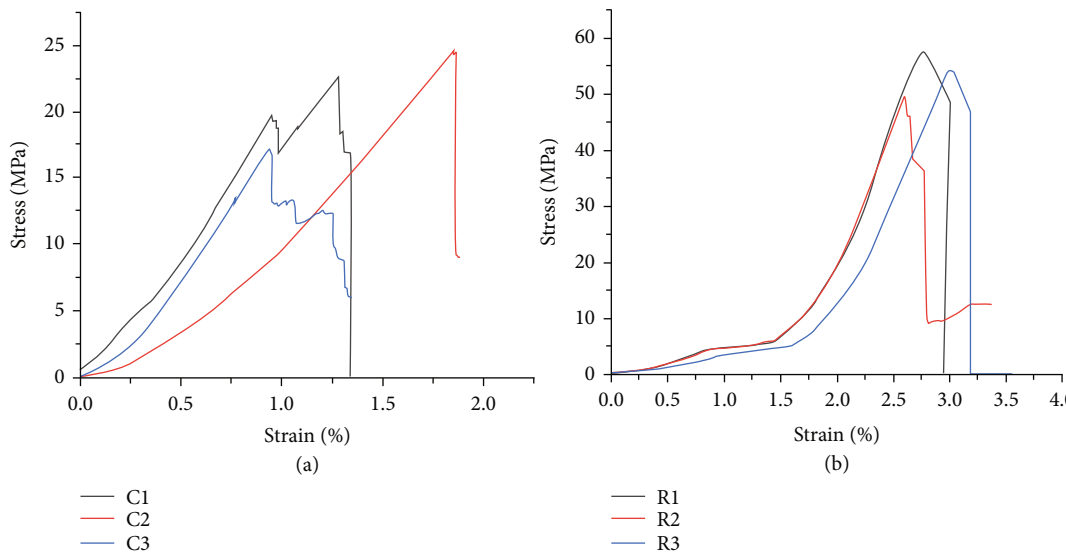

Figure 5: Mechanical behaviors of specimens under static load: (a) coal; (b) rock of floor.

Table 2: Static mechanical parameters of the specimen.

Remark	Peak strength (MPa)	Average peak strength (MPa)	Modulus of elasticity (GPa)	Average modulus of elasticity (GPa)
C-D_1	22.68		2.23	
C-D_2	24.58	21.52	2.27	2.03
C-D_3	17.30		1.59	
R-D_1	56.30		11.58	
R-D_2	52.44	54.61	12.29	12.15
R-D_3	55.09		12.59	

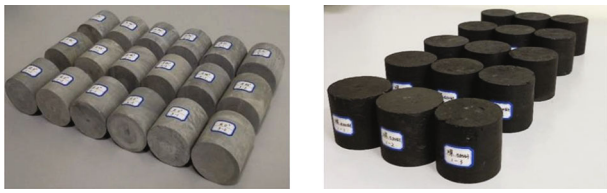

Figure 6: The specimens of coal and rock.

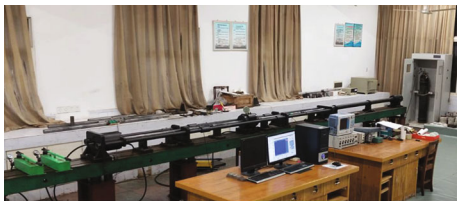

Figure 7: Split Hopkinson pressure bar test system.

4. Numerical Analysis on Surrounding Rock Behavior Evolution under Mining Influence

In this study, the FLAC3D three-dimensional model was established for numerical simulation, the retreat mining of the longwall panel was simulated, and the simulation of the caving zone of the gob was realized by combining the double-yield model.

4.1. Model Description. A numerical model that encompasses the two longwall panels, the headentry of panel 3101 and panel 3103, and the coal pillar has been built, as shown in Figure 9. The model has dimensions of 350 m in length, 275 m in width, and 138 m in height. The bottom and perimeter of the model use fixed boundaries. The fixed boundary in the y-direction is 50 m away from the open cut and the mining terminal line, respectively [18]. Among them, the longwall panel is arranged along the strike direction. Both panels are 200 m long in strike and 100 m long in inclination, and the direction of mining is as shown in the figure. In order to facilitate the analysis of the deformation evolution and plastic failure of the surrounding rock, a monitoring segment is arranged in the headentry (2) of panel 3103, and the position of the monitoring segment is 70 m away from the mining terminal line. In order to obtain the distribution characteristics of the in situ stress of the panel, the in situ stress test was carried out on the headentry (2) with a hollow inclusion meter. The results show that the vertical stress in the z-direction is 22.77 MPa, the horizontal stress in the x-direction is 21.93 MPa, and the horizontal stress in the y-direction is 16.44 MPa. This result is approximated and simplified, and the boundary conditions of the model

Table 3: Dynamic test scheme.

	Coal remark	Rock remark	Dimensions (height × diameter) (mm)	Impact pressure (MPa)
SHPB impact dynamic load test	C-D_1	R-D_1	50 × 50	0.45
	C-D_2	R-D_2	50 × 50	0.50
	C-D_3	R-D_3	50 × 50	0.55

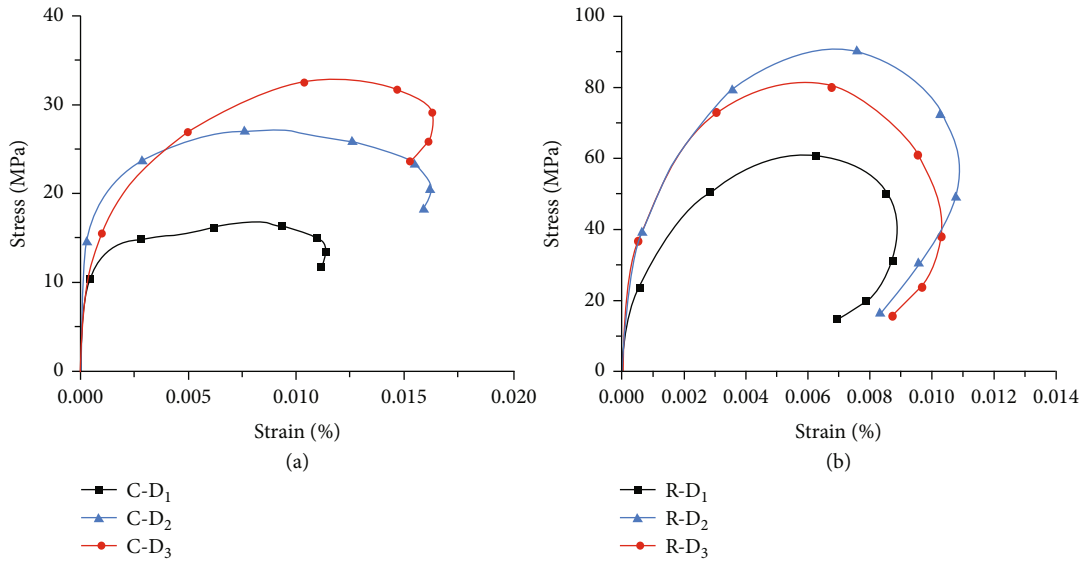

Figure 8: Mechanical behaviors of specimens under impact dynamic load: (a) coal; (b) rock of floor.

Table 4: Dynamic mechanical parameters of the specimen.

Remark	Impact pressure (MPa)	Dynamic strength (MPa)	Strain rate (s^{-1})	Peak strain (%)
C-D_1	0.45	16.80	11.97	0.00783
C-D_2	0.50	27.11	17.75	0.00824
C-D_3	0.55	32.95	20.91	0.01194
R-D_1	0.45	60.93	34.14	0.00589
R-D_2	0.50	81.35	47.27	0.00570
R-D_3	0.55	90.70	52.26	0.00683

are finally determined. Assuming that the unit weight of the overlying is 0.025 MN/m^3, the top boundary of the model is loaded with a vertical stress of 16.9 MPa, and the pressure of the overburden pressure is simulated. The stress applied in the x- and y-direction of the model is 1.3 times the vertical stress, and the gravitational acceleration is taken as 9.8 m/s^2. The mechanical properties of coal and rock mass are shown in Table 5, which is estimated from the intact rock properties using the Hoek-Brown failure criterion [19].

The model is defined as a strain softening model, and this model has been widely accepted for the simulation of underground coal mines [20, 21]. In the numerical simulation, the consolidation behavior of the gob must be considered in order to simulate real engineering conditions. The double-yield model embedded in FLAC3D is a well-accepted approach for simulating the mechanical behavior of gob under compaction [22, 23]. According to the actual mining sequence, the panel 3101 is firstly mined in a distributed manner, and the gob is filled with a double-yield model after 10 m behind the longwall panel. After the panel 3101 is mined, the headentry (2) of panel 3103 is excavated, and the support is followed by the excavation. The support simulation of the entry is realized by using structural elements such as built-in cables [24], and the support design used is the same as the field application support scheme, as shown in Figure 10. Both rebar and cable bolts are partially grouted with resin cartridges, and the relevant mechanical parameters are shown in Table 6. For the convenience of presentation, only the support of the 2 m section of the entry is shown. After the entry excavation is completed, the retreat mining of the panel 3103 is carried out, and the stress environment, plastic zone, and deformation evolution characteristics of the entry floor during the mining are studied.

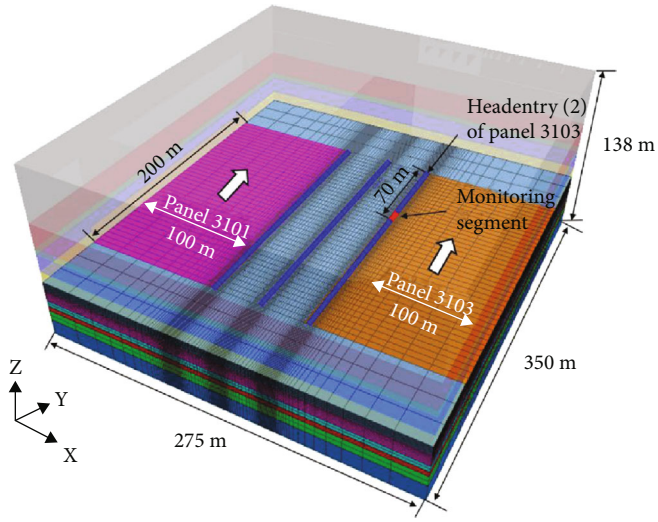

Figure 9: Numerical model layout.

Table 5: The mechanical properties of coal and rock mass of modeled materials.

Lithology	K (GPa)	G (GPa)	ρ (kg/m^3)	φ (°)	c (MPa)	σ_t (MPa)
Fine sandstone	3.92	2.35	2570	38	3.63	0.92
Medium sandstone	4.01	2.76	2560	39	3.99	1.10
Pebblestone	2.79	2.09	2660	40	5.02	0.85
Fine sandstone	3.32	1.992	2570	36	3.24	0.24
Sandy mudstone	2.24	2.05	2724	32	2.7	0.38
3-1 coal	3.21	0.68	1851	32	2.22	0.31
Sandy mudstone	4.71	1.57	2463	30	2.40	0.46
Fine sandstone	2.58	2.33	2560	32	2.6	0.38
Mudstone	4.71	1.57	2463	30	2.40	0.46
Fine sandstone	9.6	7.13	2720	37	4.13	1.05
Sandy mudstone	4.28	2.05	2365	33	3.12	1.31

K is the bulk modulus, G is the shear modulus, c is the cohesion, σ_t is the tensile strength, φ is the friction angle, and ρ is the density.

4.2. Analysis on Evolution of Mechanical Response of Surrounding Rock during Mining

4.2.1. The Stress Evolution of the Floor under the Influence of Mining. The deformation and failure of the entry are closely related to the transfer and redistribution of the surrounding rock stress; especially in the deep high-stress environment, the spatial distribution and evolution of the stress have a significant impact on the deformation and failure characteristics [25, 26]. For mines where floor rockburst is the main manifestation, analyzing the evolution of floor stress under the influence of mining will help to further grasp its inherent disaster mechanism.

(1) Evolution of Vertical Stress of the Floor. When the panel 3103 is mined forward by 30 m, 60 m, 90 m, and 120 m, the vertical stress distribution of the floor is shown in Figure 11. It can be seen that as the panel is gradually mined forward, the internal stress of the surrounding rock is readjusted and distributed. In front of the panel and in the coal pillar on the left side of the headentry (2), there is a vertical stress concentration area, that is, the advanced support abutment pressure area. The rock mass in the caving zone in the gob behind the panel is gradually compacted under the action of the overlying strata, and the phenomenon of pressure relief and stress recovery occurs. As the mining distance of the panel increases, the vertical stress in the gob increases gradually.

A stress measuring line is arranged along the mining direction of the panel at the coal pillar to monitor the vertical stress in the stress concentration area, as shown in Figure 12. Combining with Figure 11, it can be seen that the mining distance has a significant influence on the vertical stress concentration distribution of the coal pillar. When the panel is mined by 30 m, the stress distribution in the coal pillar is uniform, and there is no obvious stress concentration. When the panel is mined by 60 m, stress concentration begins to appear at 5-15 m in front of the panel, the stress peak at 10 m is about 40.4 MPa, and the stress concentration coefficient is 2.39. When the panel is mined by 90 m, the

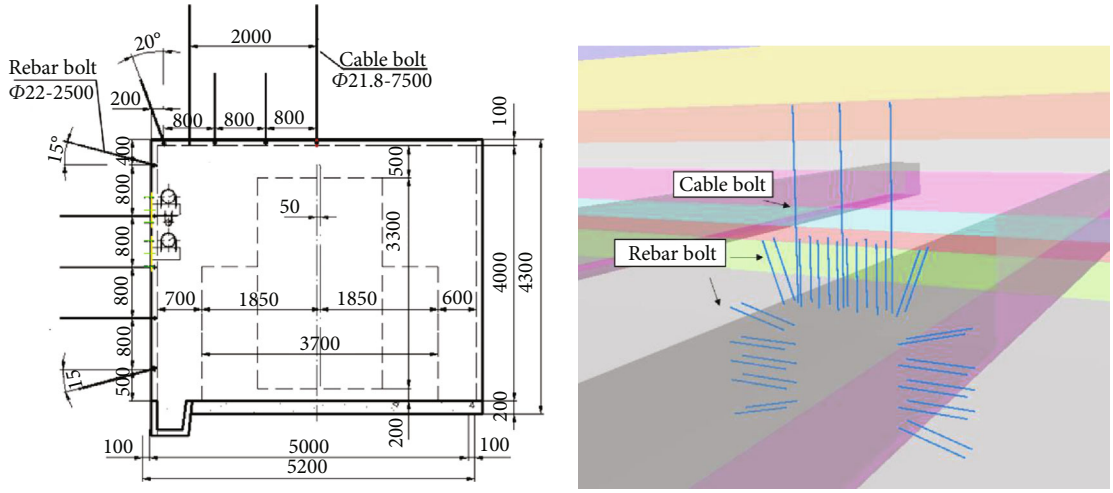

(a) (b)

Figure 10: Design and numerical simulation of entry support design: (a) entry support design; (b) simulation of entry support design.

Table 6: The structural elements of mechanical parameters.

Type	L (mm)	L_r (mm)	D (mm)	F_t (KN)
Rebar bolt	2500	1250	22	225
Cable bolt	7500	2500	21.8	510

L is the length of the structural element, L_r is the resin grout length, D is the diameter, and F_t is the tensile strength.

degree of stress concentration deepens, the peak stress is about 43.5 MPa, and the stress concentration coefficient reaches 2.57. When the panel is mined by 120 m, the range of stress concentration is further expanded, the peak stress is about 52.7 MPa, and the stress concentration coefficient is 3.11. As the mining distance of the panel increases, the vertical stress concentration formed in the coal pillar on the left side of the headentry (2) increases gradually. The peak of the advanced abutment pressure of the panel gradually moves forward, and the range of concentrated stress also increases. Considering engineering practice, the high stress concentration of surrounding rock in such coal pillars will often lead to the accumulation of high strain energy, which in turn causes the sudden release of high strain energy to induce dynamic failure of surrounding rock [27].

(2) Evolution of Horizontal Stress of the Floor. When the panel 3103 is mined forward by 30 m, 60 m, 90 m, and 120 m, the horizontal stress distribution of the floor is shown in Figure 13. It can be seen that the horizontal stress distribution at the roadway floor is similar, and they are all high-level stress concentrations. As the panel is mined gradually, the stress of the surrounding rock is readjusted and distributed. The panel floor is affected by the overlying rock collapse in the previous gob, and the stress remains at a relatively small level, but it also shows the same evolution as the vertical stress. When the panel is mined by 30 m, there is a small range of horizontal stress concentration on the headentry (2) floor 17-27 m ahead of the panel, and the stress peak reaches 30.8 MPa. When the panel is mined by 60 m, the range of concentrated stress is reduced, but the peak of horizontal stress still reaches 30 MPa. When the panel is mined by 90 m, the range of the concentrated stress remains unchanged, and the peak of the horizontal stress is reduced to 29 MPa. When the panel is mined by 120 m, there is no obvious peak of horizontal stress, and the horizontal stress is all about 28 MPa. The horizontal stress of the floor is less affected by the panel mining, but the floor is in a high-level stress environment for a long time, which is prone to the phenomenon of high strain energy accumulation in the surrounding rock. At the same time, the influence of "creep effect" on the floor will be further enhanced [28, 29], and its rock mass properties will be weakened, which increases the possibility of floor rockburst.

(3) Evolution of Maximum Principal Stress of the Floor. The distribution and evolution of the maximum principal stress of the floor under different mining distances of the panel are further analyzed. A cross-sectional view of the coal pillar on the left side of the headentry (2) is cut along the mining direction of the panel, and the stress evolution of the maximum principal stress with the panel mining is drawn, as shown in Figure 14. It can be seen that as the panel is mined forward, the maximum principal stress accumulation of the floor continues to intensify. When the panel is mined by 30 m, the maximum principal stress of the roof and floor is not significantly concentrated. When the panel is mined by 60 m, the stress concentration begins to appear at 10 m in front of the panel and 2 m from the entry floor, and the stress peak is about 51.1 MPa. When the panel is mined by 90 m, the stress concentration at the same distance ahead of the panel intensifies, the range expands, and the stress peak is about 56.0 MPa. When the panel is mined by 120 m, the stress concentration of the floor is further improved, and the range is also expanded from the original position to the direction away from the panel.

The stress measuring line is arranged near the coal pillar 10 m from the front of the panel and 2 m from the headentry (2) floor, and the maximum principal stress distribution

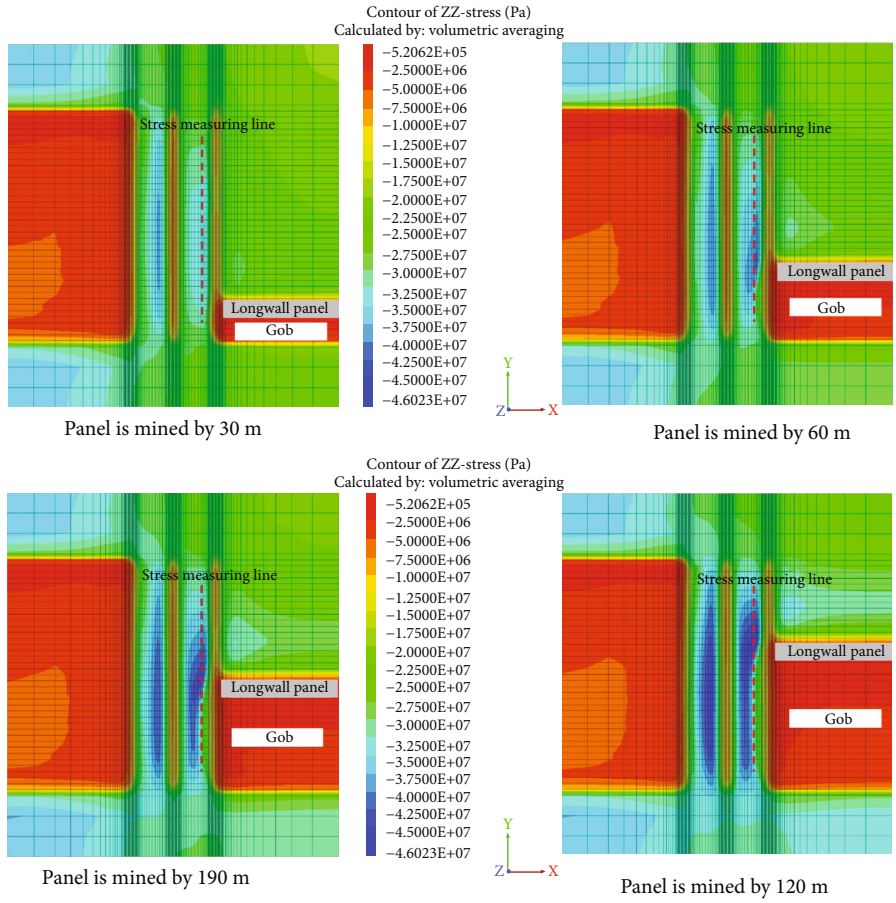

Figure 11: The vertical stress distribution of the floor with different mining distances.

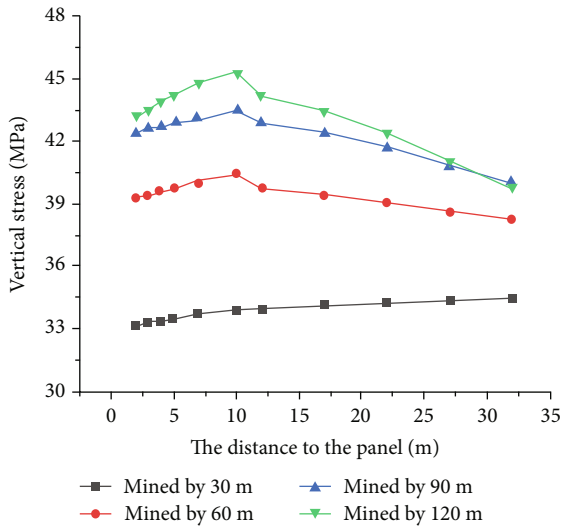

Figure 12: The vertical stress distribution curve of the stress measuring line.

curve of the stress measuring line is drawn, as shown in Figure 15. Comparing the three curves when the panel is mined by 60 m, 90 m, and 120 m, the distribution trends are similar and the values all increase. When the panel is mined from 30 m to 60 m, the maximum principal stress increases the most, with an average increase of about 5 MPa. When the panel is mined from 60 m to 120 m, the growth rate decreases, and the decline rate of stress near the maximum principal stress peak increases.

In summary, the stress environment of the panel entry and adjacent coal pillar floor is poor, which is significantly affected by mining and has rapid stress drop. The stress drop can be used to study the abutment pressure, which helps to quantitatively analyze the sudden discontinuous behavior of the rock [30]. Long-term high stress promotes the "creep effect," which in turn leads to further deterioration of the mechanical properties of the floor. Under such conditions, with the dynamic load disturbance such as the sudden rupture and instability of the roof or the uneven stress balance caused by other factors such as mining speed, it is very easy to cause the occurrence of floor rockburst.

4.2.2. The Deformation Evolution of Surrounding Rock under the Influence of Mining. To study the surrounding rock deformation of the full section of the entry during the mining, 10 displacement monitoring points are arranged in the monitoring section, as shown in Figure 16. Deformation at monitoring points is recorded during their entire service life, which begins immediately after excavation and support installation and ends when the panel is mined to the monitoring section. Such an arrangement is aimed at thoroughly

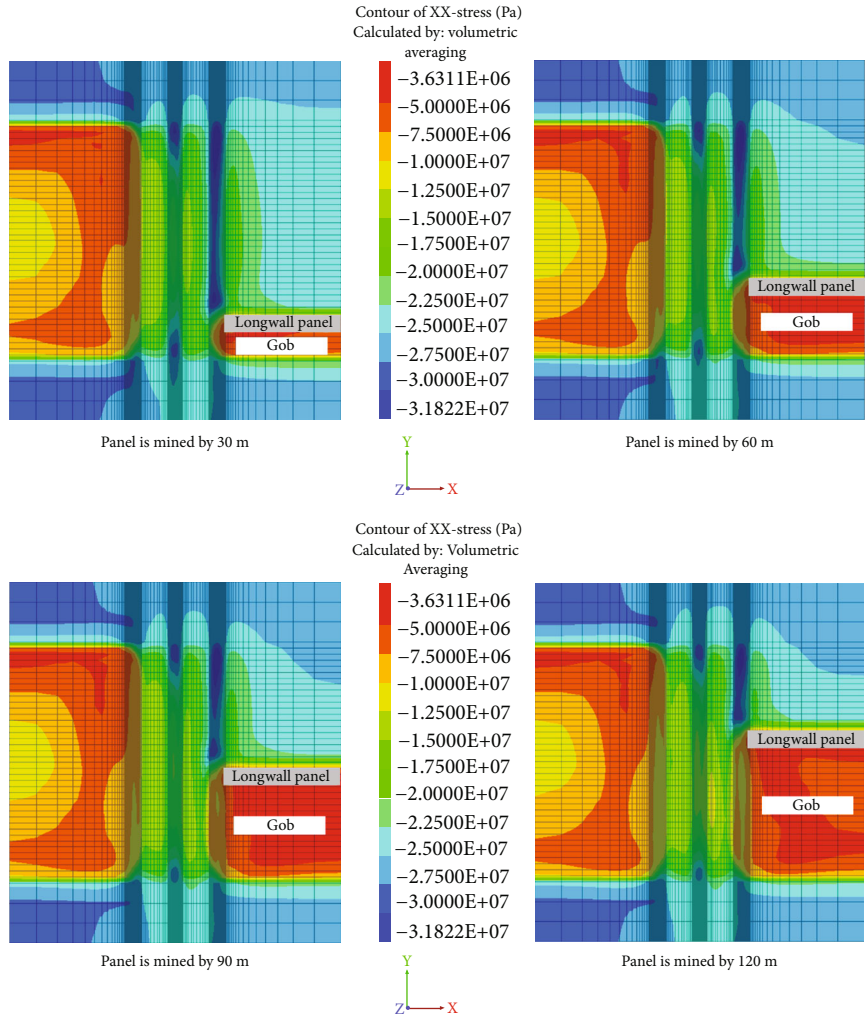

Figure 13: The horizontal stress distribution of the floor with different mining distances.

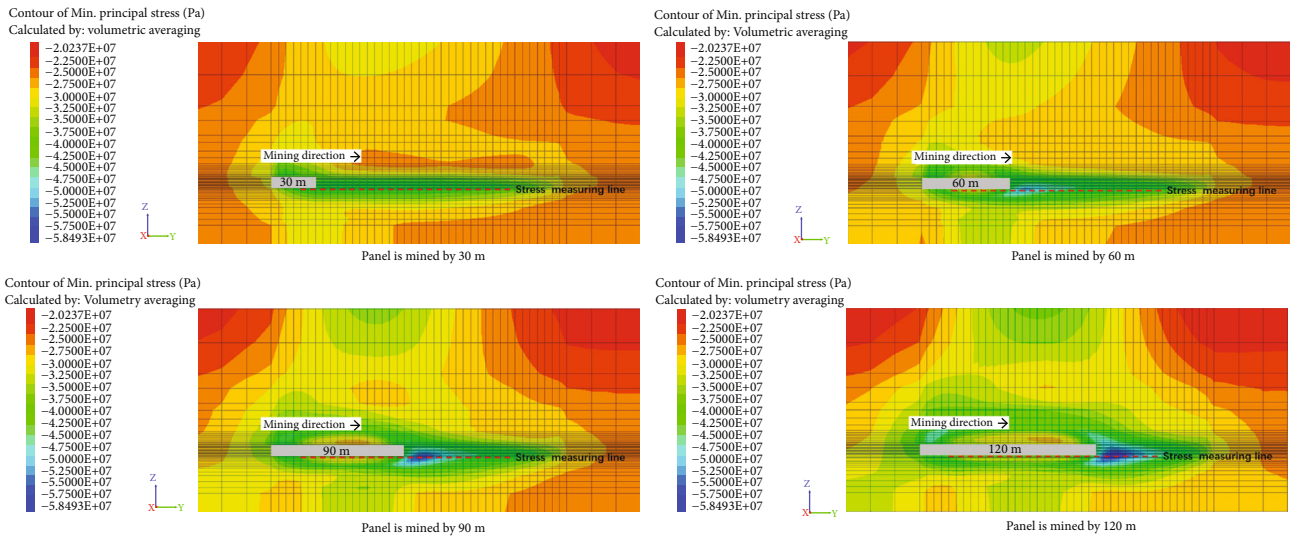

Figure 14: The maximum principal stress distribution of the floor with different mining distances.

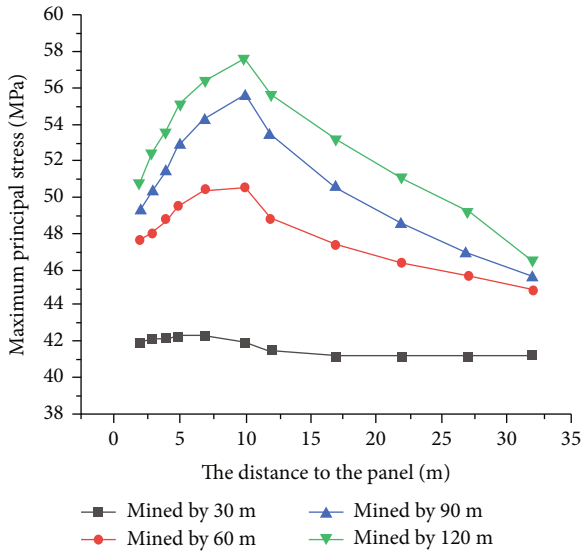

Figure 15: The maximum principal stress distribution curve of the stress measuring line.

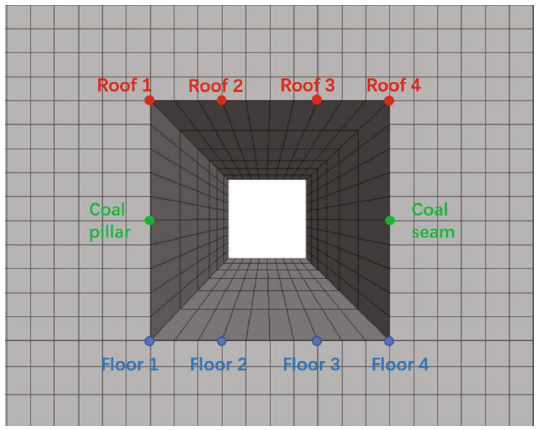

Figure 16: Layout of monitoring points.

monitoring the subsidence of the roof, convergence of ribs, and heave of the floor induced by mining.

Figure 17 shows the deformation evolution characteristics of the surrounding rock in the monitoring section under different mining distances. In the figure, "displacement" represents the amount of deformation of the entry during the entire service period, and "deformation" represents the amount of deformation of the entry since the start of the mining of the panel. It can be seen from Figures 7(a)–7(d) that the overall deformation evolution of the roof and ribs is similar, and the deformation rate is increasing. After the mining, the deformation rate of the roof and the ribs began to increase, but the growth rate is slow; when the panel is mined to 40 m from the monitoring section, the deformation rate increased significantly and was proportional to the mining distance of the panel. When the panel is mined to the monitoring section, the service life of the entry in the monitoring section will be terminated. At this time, the maximum deformation of the roof and the ribs is about 572 mm and 516 mm, respectively. The maximum deformations affected by mining are 197 mm and 173 mm, accounting for 34.4% and 33.5% of the total deformation. Comparing the deformation patterns of the roof and ribs during the mining, the roof sinks uniformly and symmetrically, and the deformation rate of each monitoring point is the same. The ribs show that the side of the coal seam is more significantly affected by the mining. With the mining of the panel, the deformation rate of the side of the coal seam is greater than that of the coal pillar.

It can be seen from Figures 7(e) and 7(f) that the deformation evolution of the floor is different from that of the roof and the ribs. As the mining progresses at each monitoring point of the floor, the overall deformation shows a trend of a slight decrease at first and then a rapid increase. During the distance from the mining panel to the monitoring section from 110 m to 30 m, affected by the overall subsidence of the stratum, the floor angles on the left and right sides slowly sink. And the heave of the floor was reduced; the maximum reduction amounted to 14 mm, while the heave at the two monitoring points in the middle remained unchanged basically. From 30 m to 0 m, the deformation rate accelerated, and the heave of the floor at each monitoring point increased nonlinearly and suddenly. The maximum deformation of the floor is 341 mm, of which the maximum deformation caused by mining is 142 mm, accounting for 41.6% of the total deformation. The heave of the floor is mainly near the centerline, and the deformation of the floor angles is small.

In conclusion, the surrounding rock deformation of the entry floor is more sensitive to panel mining. When the panel is far away from the monitoring section, the deformation of the surrounding rock is dominated by the slow subsidence of the roof and the horizontal movement of the ribs, and the floor is not deformed basically. The surrounding rock has the characteristics of long continuous deformation and stable growth rate. When the panel is mined to the vicinity of the monitoring section, the "mutation" characteristic of the floor heave of the panel entry is apparent, and the deformation rate of the floor increases rapidly and is higher than that of the roof and ribs.

4.2.3. The Plastic Failure Evolution of Surrounding Rock under the Influence of Mining. After the entry is excavated, the state of original stress is broken, which makes the surface of the entry and the shallow surrounding rock prone to plastic failure and converges into the roadway space. Therefore, the expansion range of the plastic zone can be used as an effective index to measure the stability of the surrounding rock of the entry. Figure 18 shows the distribution of the plastic zone in the monitoring section under different mining distances. It can be seen that when the panel is mined from 30 m to 60 m, the range of the plastic zone of the roof, floor, and coal pillars remains basically unchanged, the plastic zone of the coal seam extends to the deep, and the damage degree expands from 3.5 m to 4.3 m, an increase of 22.8%. When the panel is mined from 60 m to 90 m, the range of the roof and floor remains unchanged, and the damage degree of the coal pillar expands from 4.1 m to 4.9 m, an increase of 19.5. When the panel is mined from 90 m to 120 m, the range of the coal pillar and coal seam is

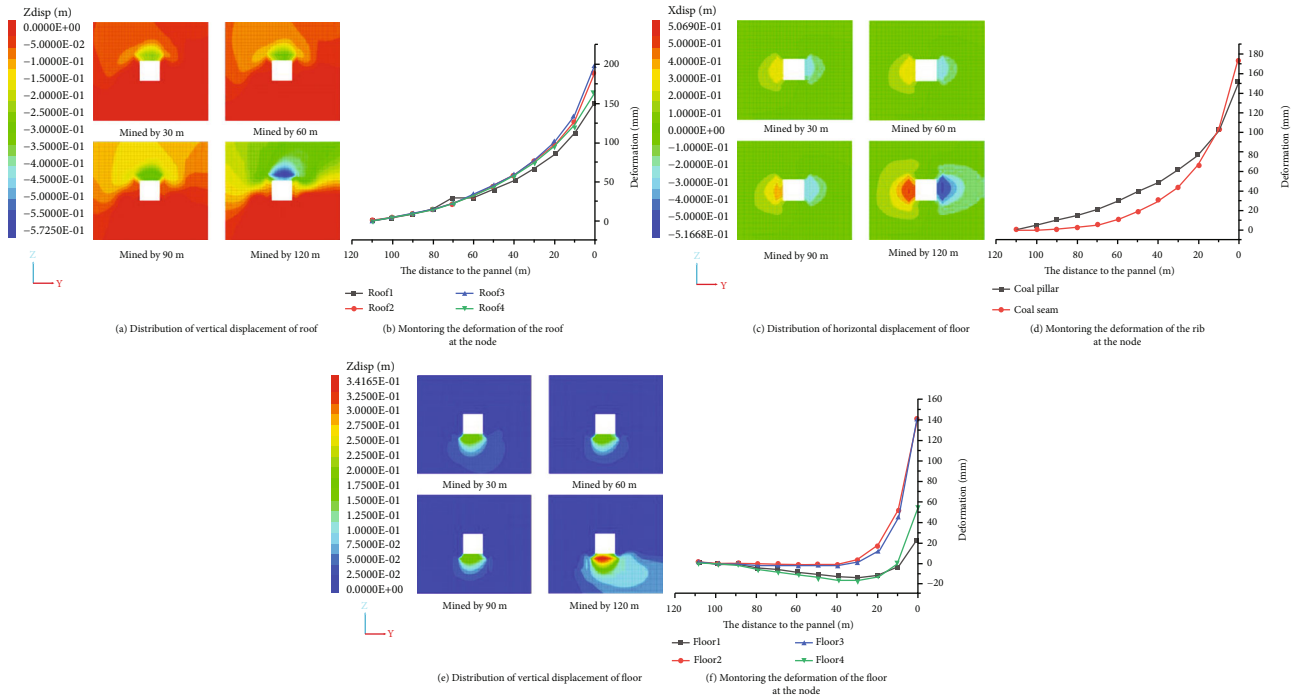

Figure 17: Deformation evolution of surrounding rock in the monitoring section with different mining distances.

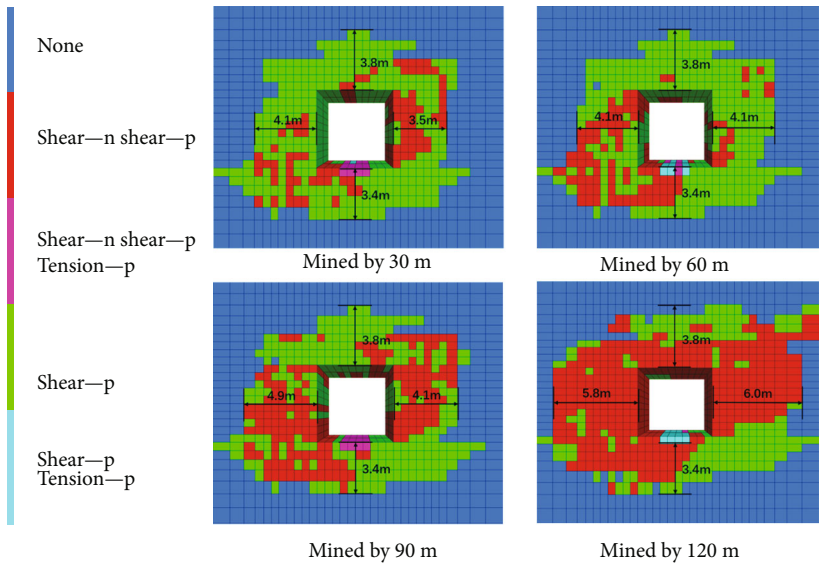

Figure 18: Distribution of the plastic failure zone in the monitoring section with different mining distances.

larger and the distribution is wider. The damage degree of the coal pillar expanded from 4.9 m to 5.8 m, an increase of 18.3%, and the damage degree of the coal seam expanded from 4.1 m to 6.0 m, an increase of 46.3%. The failure damage of the roof and floor are further increased, and the overall failure trend is inclined to the mining side.

The results show that under the influence of mining, the range of the plastic zone of the ribs expands, and the range of the roof and floor remains basically unchanged. The entry and the longwall panel cut the coal seam to form an isolated coal body. Under the combined action of self-weight stress and tectonic stress, the clamping effect of the coal body is enhanced, thereby accumulating higher energy and forming a high-stress isolated coal body. With the mining of the panel, the mining-induced stress concentration of the coal body increases, and the mechanical properties of the local coal body are weakened. The high abutment pressure of the coal pillar propagates in the floor, further exacerbating the stress condition of the floor.

4.3. Field Validation. In order to validate the numerical results, a field test has been carried out at the headentry

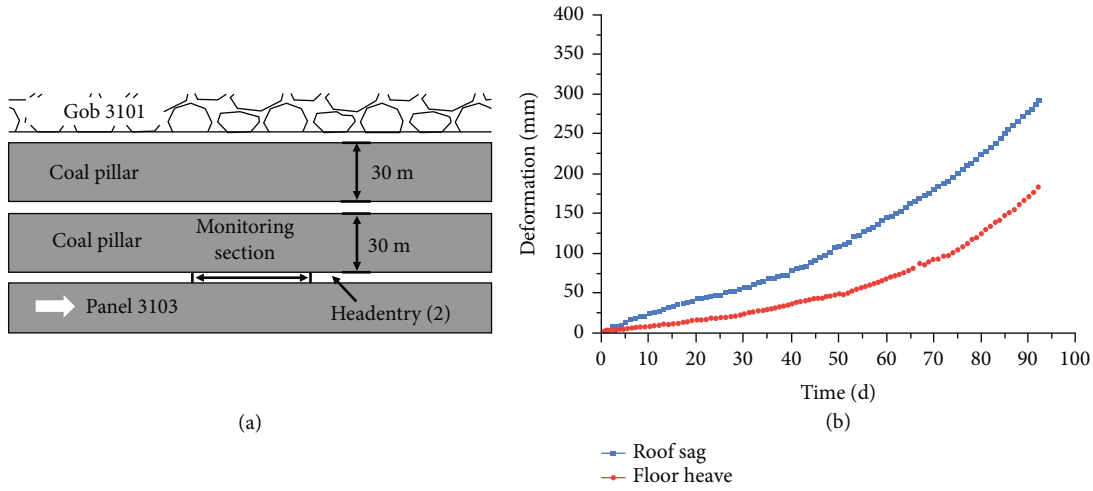

FIGURE 19: Field validation: (a) plan view of the testing site; (b) data of the monitoring station.

(2) of panel 3103, as illustrated in Figure 19(a). Multiple deformation monitoring stations have been built in a monitoring section, and average deformation of the monitoring data is shown in Figure 19(b). Note that the deformation data starts from the beginning of the retreat mining of panel 3103. Since the station monitors the variation during the monitoring time instead of the total deformation, it is more reliable to analyze the deformation rate. The results show that the deformation of the roof and floor is small, and the deformation rate of the floor has an increasing trend. In the early stage of monitoring, the rate of roof sag (1.9-2.3 mm/d) is higher than the rate of floor heave (0.9-1.3 mm/d), but in the late stage of monitoring, the rate of floor heave is consistent with it (5.8-6.7 mm/d). The field monitoring results suggest that the deformation amount of entry is small and the deformation rate of the floor increases rapidly.

While these results are not directly comparable with the numerical results, they are still consistent with the trend obtained from numerical simulation and hence serve to validate the model. In addition, it should be noted that it is extremely difficult to directly simulate the rockburst phenomenon with the finite difference method, but the numerical analysis on the surrounding rock behaviors under the effect of retreat mining is still essential for the rockburst potential analysis in this presented case.

5. Discussion on the Rockburst Mechanism of Panel 3103

The mechanical properties of the surrounding rock and the stress environment of the deep entry determine that its own stability is more sensitive to external influences than the shallow ones [31]. Whether it is the mining activity under the near-field condition or the dynamic load disturbance under the far-field condition, it will inevitably affect the coal-rock mass system around the entry [32]. Combined with the laboratory test, numerical simulation, and field practice, the rockburst of the headentry (2) of the panel 3103 occurred repeatedly during the mining; its reasons are as follows.

First of all, the overlying rock layers on the panel are mostly coarse/medium sandstone with a thickness of 25-58 m. There is no weak rock layer between the multilayer sandstones, and the formed composite hard and thick rock layer is not easy to collapse, and it is easy to form a large-area cantilever roof structure. In addition, the unreasonable coal pillars between adjacent panel 3101 leave the coal and rock mass around the panel in a state of high abutment pressure, and the abutment pressure has a large influence range. The occurrence of rockburst is the result of multiple factors, but it is undeniable that the nature of surrounding rock is the most basic and most important factor. Based on the results obtained in the laboratory tests, the tendency for rockburst to occur can be further clarified. The uniaxial compressive test shows that the coal and rock mass near the panel has brittle characteristics, and the floor rock is harder and stronger than the coal seam. This provides mechanical conditions for the accumulation and transfer of energy [33–35]. The SHPB impact dynamic load test shows that the strength of coal and rock mass under dynamic load is higher than that under static load. In particular, the dynamic strength of the floor rock under each impact pressure is larger than that of the coal. This indicates that the floor rock mass is more sensitive to dynamic load disturbance. Under the influence of high horizontal stress, the floor accumulates more elastic energy. When receiving the external disturbance, the horizontal stress of the floor of the entry increases instantaneously to reach the failure strength of the floor rock. If the floor structure cannot resist the horizontal extrusion, a large amount of floor heave will be generated. Secondly, affected by the mining of the adjacent panel, the stress in the surrounding rock of the entry and the advanced abutment pressure of the panel are superimposed, resulting in a further increase in the stress concentration and the deterioration of the stress environment of the surrounding rock. The long-term high-stress environment increases the "creep effect" on the coal and rock mass, which in turn weakens its ability to resist external dynamic load

disturbances. In particular when the panel is mined until the strike length is equal to the inclination length, that is, the panel is square, the overlying rock movement is active [36]. The dynamic load disturbance caused by the fracture and caving of the overlying strata makes the high stress of the entry release unevenly, which is prone to rockburst instability.

To sum up, under the influence of large burial depth, wide coal pillar, mining-induced stress, and roof breaking, the entry is in a state of high static load and strong disturbance and has already met stress conditions, energy conditions, and induced conditions for rockburst. In the structure of "roof-rib-floor" of the entry, the floor has no support, which provides a weak surface and space for the concentrated release of energy. Once the energy accumulated in the floor reaches the critical value of rockburst instability, the stress balance of the surrounding rock of the entry is broken, prompting the sudden release of the high elastic energy of the floor, which will lead to dynamic disasters such as rockburst. Based on the above analysis, the accumulation of high stress and dynamic disturbance should be avoided. In the follow-up prevention and control, it can be considered from the pressure relief of the roof and coal by drilling, improving the layout of the entry, and strengthening the floor.

6. Conclusion

(1) The mechanical properties of the coal and rock mass near the panel were obtained based on the laboratory tests under different dynamic and static load conditions. The results show that the floor rock has high compressive strength and brittle characteristics. Under the action of impact dynamic load, its dynamic strength is positively correlated with impact pressure, and the high elastic energy accumulation and high-stress transfer of hard rock provide the mechanical premise for rockburst

(2) Based on the numerical simulation of panel mining, under the influence of wide coal pillars and panel mining, the floor stress of entry presents the characteristics of large-scale and high accumulation. The vertical stress and the maximum principal stress of the floor are concentrated in the coal pillar along the entry, and the horizontal stress is concentrated in the entry floor, and the degree of each stress concentration increases with the panel mining. During the mining of the panel, the deformation rate of the roof and the ribs of the entry is stable, while the floor has the phenomenon of rapid heave of floor. The range of the plastic zone in the ribs is significantly affected by mining and gradually expands to the deep part of the surrounding rock

(3) The entry under high stress is more sensitive to external disturbance, and the weak links of the surrounding rock system are more easily damaged. With the engineering disturbance and roof breaking caused by the panel mining, the system was affected by the strong dynamic load disturbance. The floor lacks pressure relief and support means, which often becomes a breakthrough for rockburst. Once the limit equilibrium state of the floor is broken, sudden instability will occur, which will lead to the rockburst of the floor

Data Availability

Data used to support the results of this study can be found in this manuscript text.

Conflicts of Interest

The authors declare that they have no known competing financial interests or personal relationships that could have appeared to influence the work reported in this paper.

Acknowledgments

This study was financially supported by the National Natural Science Foundation of China (52074166) and National Natural Science Foundation of Shandong Province (ZR2021YQ38) and the Open Grant of State Key Laboratory of Mining Response and Disaster Prevention and Control in Deep Coal Mines (SKLMRDPC20KF02).

References

[1] H. P. Xie, F. Q. Gao, and Y. Ju, "Research and development of rock mechanics in deep ground engineering," *Chinese Journal of Rock Mechanics and Engineering*, vol. 34, no. 11, pp. 2161–2178, 2015.

[2] K. G. Zheng, Y. Liu, T. Zhang, and J. Zhu, "Mining-induced stress control by advanced hydraulic fracking under a thick hard roof for top coal caving method: a case study in the Shendong mining area, China," *Minerals*, vol. 11, no. 12, p. 1405, 2021.

[3] Q. Sun, J. X. Zhang, Q. Zhang, and X. Zhao, "Analysis and prevention of geo-environmental hazards with high-intensive coal mining: a case study in China's western eco-environment frangible area," *Energies*, vol. 10, no. 6, p. 786, 2017.

[4] Y. D. Jiang, Y. S. Pan, F. X. Jiang, L. M. Dou, and Y. Ju, "State of the art review on mechanism and prevention of coal bumps in China," *Journal of China Coal Society*, vol. 39, no. 2, pp. 205–213, 2014.

[5] L. M. Dou, Z. L. Mu, Z. L. Li, A. Y. Cao, and S. Y. Gong, "Research progress of monitoring, forecasting, and prevention of rockburst in underground coal mining in China," *International Journal of Coal Science and Technology*, vol. 1, no. 3, pp. 278–288, 2014.

[6] N. G. W. Cook, E. P. Hoek, J. P. G. Pretorius, W. D. Ortlepp, and M. D. G. Salamon, "Rock mechanics applied to the study of rockbursts," *Journal of the South African Institute of Mining and Metallurgy*, vol. 66, no. 10, pp. 435–528, 1965.

[7] Z. T. Bieniawski, H. G. Denkhaus, and U. W. Vogler, "Failure of fractured rock," *International Journal of Rock Mechanics & Mining Sciences & Geomechanics Abstracts*, vol. 6, no. 3, pp. 323–341, 1969.

[8] I. M. Petukhov and A. M. Linkov, "The theory of post-failure deformations and the problem of stability in rock mechanics," *International Journal of Rock Mechanics & Mining Sciences & Geomechanics Abstracts*, vol. 16, no. 2, pp. 57–76, 1979.

[9] I. Vardoulakis, "Rock bursting as a surface instability phenomenon," *International Journal of Rock Mechanics & Mining Sciences & Geomechanics Abstracts*, vol. 21, no. 3, pp. 137–144, 1984.

[10] H. P. Xie and W. G. Pariseau, "Fractal character and mechanism of rock bursts," *International Journal of Rock Mechanics & Mining Sciences & Geomechanics Abstracts*, vol. 12, no. 1, pp. 28–37, 1993.

[11] Q. Qi, Y. Pan, H. Li et al., "Theoretical basis and key technology of prevention and control of coal-rock dynamic disasters in deep coal mining," *Journal of China Coal Society*, vol. 45, no. 5, pp. 1567–1584, 2020.

[12] D. H. Song, E. Y. Wang, N. Li, M. Jin, and S. Xue, "Rock burst prevention based on dissipative structure theory," *International Journal of Mining Science and Technology*, vol. 22, no. 2, pp. 159–163, 2012.

[13] Y. Pan, "Disturbance response instability theory of rockburst in coal mine," *Journal of China Coal Society*, vol. 43, no. 8, pp. 2091–2098, 2018.

[14] J. R. Cao, L. M. Dou, G. G. Zhu, J. He, S. Wang, and K. Zhou, "Mechanisms of rock burst in horizontal section mining of a steeply inclined extra-thick coal seam and prevention technology," *Energies*, vol. 13, no. 22, p. 6043, 2020.

[15] H. P. Kang, J. F. Lou, F. Q. Gao, J. Yang, and J. Li, "A physical and numerical investigation of sudden massive roof collapse during longwall coal retreat mining," *International Journal of Coal Geology*, vol. 188, pp. 25–36, 2018.

[16] K. Holub, J. Rušajová, and J. Holečko, "Particle velocity generated by rockburst during exploitation of the longwall and its impact on the workings," *International Journal of Rock Mechanics & Mining Sciences*, vol. 48, no. 6, pp. 942–949, 2011.

[17] G. Zhou, T. Xu, H. Konietzky et al., "An improved grain-based numerical manifold method to simulate deformation, damage and fracturing of rocks at the grain size level," *Engineering Analysis with Boundary Elements*, vol. 134, no. 1, pp. 107–116, 2022.

[18] L. S. Jiang, P. Kong, J. M. Shu, and K. Fan, "Numerical analysis of support designs based on a case study of a longwall entry," *Rock Mechanics and Rock Engineering*, vol. 52, no. 9, pp. 3373–3384, 2019.

[19] E. Hoek and E. T. Brown, "Practical estimates of rock mass strength," *International Journal of Rock Mechanics & Mining Sciences*, vol. 34, no. 8, pp. 1165–1186, 1997.

[20] P. Wang, L. S. Jiang, J. Q. Jiang, P. Zheng, and W. Li, "Strata behaviors and rock burst-inducing mechanism under the coupling effect of a hard, thick stratum and a normal fault," *International Journal of Geomechanics*, vol. 18, no. 2, article 04017135, 2018.

[21] G. C. Zhang, S. J. Liang, Y. L. Tan, F. Xie, S. Chen, and H. Jia, "Numerical modeling for longwall pillar design: a case study from a typical longwall panel in China," *Journal of Geophysics and Engineering*, vol. 15, no. 1, pp. 121–134, 2018.

[22] Z. Zhang, C. J. Bai, Y. Chen, and S. Yan, "An innovative approach for gob-side entry retaining in highly gassy fully-mechanized longwall top-coal caving," *International Journal of Rock Mechanics & Mining Sciences*, vol. 80, pp. 1–11, 2015.

[23] E. Esterhuizen, C. Mark, P. R. Engineer, M. Engineer, and M. M. Murphy, "Numerical model calibration for simulating coal pillars, gob and overburden response," in *Proceedings of the 29th International Conference on Ground Control in Mining*, pp. 45–67, Morgantown, West Virginia University, 2010.

[24] L. S. Jiang, P. P. Zhang, L. J. Chen et al., "Numerical approach for goaf-side entry layout and yield pillar design in fractured ground conditions," *Rock Mechanics and Rock Engineering*, vol. 50, no. 11, pp. 3049–3071, 2017.

[25] S. Peng, *Coal Mine Ground Control*, Peng SS Publisher, Morgantown, WV, USA, 3rd edition, 2008.

[26] B. Chen, "Stress-induced trend: the clustering feature of coal mine disasters and earthquakes in China," *International Journal of Coal Science & Technology*, vol. 7, no. 4, pp. 676–692, 2020.

[27] W. F. Li, J. B. Bai, S. Peng, X. Wang, and Y. Xu, "Numerical modeling for yield pillar design: a case study," *Rock Mechanics and Rock Engineering*, vol. 48, no. 1, pp. 305–318, 2015.

[28] J. C. Innocente, C. Paraskevopoulou, and M. S. Diederichs, "Estimating the long-term strength and time-to-failure of brittle rocks from laboratory testing," *International Journal of Rock Mechanics and Mining Sciences*, vol. 147, article 104900, 2021.

[29] N. Golsanami, M. N. Jayasuriya, W. Yan et al., "Characterizing clay textures and their impact on the reservoir using deep learning and Lattice-Boltzmann simulation applied to SEM images," *Energy*, vol. 240, article 122599, 2022.

[30] D. J. Xue, J. Zhou, Y. T. Liu, and L. Gao, "On the excavation-induced stress drop in damaged coal considering a coupled yield and failure criterion," *International Journal of Coal Science & Technology*, vol. 7, no. 1, pp. 58–67, 2020.

[31] M. Zhang and F. X. Jiang, "Rock burst criteria and control based on an abutment-stress-transfer model in deep coal roadways," *Energy Science and Engineering*, vol. 8, no. 8, pp. 2966–2975, 2020.

[32] S. K. Zhang, L. Lu, Z. M. Wang, and S. D. Wang, "A physical model study of surrounding rock failure near a fault under the influence of footwall coal mining," *International Journal of Coal Science & Technology*, vol. 8, no. 4, pp. 626–640, 2021.

[33] K. Bo-Hyun, W. Gabriel, M. K. Larson, and S. Berry, "Experimental study on the confinement-dependent characteristics of a Utah coal considering the anisotropy by cleats," *International Journal of Rock Mechanics and Mining Sciences*, vol. 8, no. 2, pp. 77–87, 2021.

[34] S.-F. Wang, Y. Tang, and S.-Y. Wang, "Influence of brittleness and confining stress on rock cuttability based on rock indentation tests," *Journal of Central South University*, vol. 28, no. 9, pp. 2786–2800, 2021.

[35] S. F. Wang, L. C. Sun, X. B. Li et al., "Experimental investigation and theoretical analysis of indentations on cuboid hard rock using a conical pick under uniaxial lateral stress," *Geomechanics and Geophysics for Geo-Energy and Geo-Resources*, vol. 8, no. 1, article 34, 2022.

[36] S. T. Zhu, D. C. Ge, F. X. Jiang et al., "Rock burst mechanism under coupling action of working face square and regional tectonic stress," *Shock and Vibration*, vol. 2021, Article ID 5538179, 11 pages, 2021.